Higher Order Variable Extrapolation For Unstructured Finite Volume RANS Flow Solvers

Clarence O. E. Burg*

Jackson State University, Jackson, MS 39204

A new variable extrapolation formulation for unstructured finite volume codes is developed which closely resembles the MUSCL-scheme used within structured flow solvers. This new formulation is based on information currently available to the unstructured flow solvers, namely the variable information and the gradient information, and as such, it is trivial to implement within most finite volume flow solvers. This new variable extrapolation formulation represents a one-parameter family of equations and under certain circumstances, it is fully equivalent to the MUSCL-scheme, which is also a one-parameter family. A wide variety of results are presented, including theoretical analysis of the truncation error and numerical analysis of the truncation error for a one-dimensional problem, using the method of manufactured solutions, as well as for a two-dimensional problem. Inviscid three-dimensional results are presented which demonstrate that the numerical viscosity can be greatly decreased via this formulation, and the viscous results for a variety of cases indicate that the drag is better predicted and that the vortical structures within the flow field are captured more accurately and further downstream of their origination. Finally, the observed improved convergence levels and stability of the new formulation are discussed, as well as the issues involved with extending this approach to achieve third-order spatial accuracy for 2D and 3D grids.

Nomenclature

$Q^L_{i+1/2}$	Variable extrapolated to left side of face at location $x_{i+1/2}$
Q^L_{ij}	Variable extrapolated to left side of face between nodes i and j
χ	U-MUSCL, MUSCL parameter
$\hat{r}_{ij}$	Vector between nodes i and j
$F(Q)$	Flux vector
Q	Variables
Q_i, Q_j	Variables at nodes i and j
∇Q	Gradient of Q
ϕ	Second-order flag for MUSCL scheme

I. Introduction

Both structured and unstructured gridding strategies are used for the solution of the Reynolds-averaged Navier-Stokes equations, as well as other important equations describing the physical world. Solvers for structured grids are able to take advantage of the structure in the grid to develop higher-order accurate discretization schemes, while most unstructured solvers are limited to approximately second-order spatial accuracy. However, the unstructured gridding strategies achieve a similar level of accuracy and error reduction in the overall simulation by significantly increasing the resolution in the regions of interest.

For structured solvers, obtaining higher-order accuracy involves developing stable discretizations for the interior cells as well as one-side discretizations for cells near the boundaries. In addition, appropriately

*Senior Research Associate, Northrop Grumman Center for HPC of Ship Systems Engineering, MS E-Center, Box 1400, 1230 Raymond Rd., Jackson, MS, 39204, AIAA member

higher-order metric transformation are typically required, since structured solvers typically transform the physical grid to a Cartesian equilateral grid. In order for the overall method to be n-th order accurate, each of these discretization must be n-th order. The MUSCL-scheme[1] (Monotonic Upstream-centered Scheme for Conservation Laws) is a compact scheme which is used to discretize the convective part of hyperbolic-dominated systems and has been adopted by many structured flow solvers,[2–4] to yield a stable, third-order accurate spatial discretization. In 1D, using a uniform spacing, the extrapolation to both sides of the face at location $i + 1/2$ is

$$\begin{aligned} Q^L_{i+1/2} &= Q_i + \frac{\phi}{4}\left((1-\chi)\,\Delta_- + (1+\chi)\,\Delta_+\right)_i \\ Q^R_{i+1/2} &= Q_{i+1} - \frac{\phi}{4}\left((1-\chi)\,\Delta_+ + (1+\chi)\,\Delta_-\right)_{i+1} \end{aligned} \tag{1}$$

where $(\Delta_+)_i = Q_{i+1} - Q_i$ and $(\Delta_-)_i = Q_i - Q_{i-1}$. If $\phi = 0$, then this is only a first-order scheme, but if $\phi = 1$, then a family of higher-order schemes is activated, which are at least second-order accurate for all values of χ. If $\chi = -1$, then this method is fully-upwinded. If $\chi = 1/3$, then the method is third-order accurate, resulting in a scheme that is referred to as "third-order upwind biased",[2] but contains information from the other side of the face.

For unstructured flow solvers, second-order accuracy is achieved by extrapolating from the center of the control volume to the face using the value and the gradient at the center.[5] Assuming that the values and the gradients are known at nodes i and j, then the value extrapolated to the face of the control volume is

$$Q^L_{ij} = Q_i + \nabla Q_i \cdot \frac{\hat{r}_{ij}}{2} \tag{2}$$

where $\hat{r}_{ij} = \vec{x}_j - \vec{x}_i$. For a perfect grid (i.e., uniform equilateral triangles or tetrahedra), this discretization results in a true second order spatial discretization, using either Green-Gauss or Least-Squares approach to reconstruct the gradient. However, more information is available at the face than is used in this extrapolation, namely the information at the node on the other side of the face, as is shown in Figure 1. By including this additional information, increased accuracy can be achieved for the variable extrapolation portion of the discretization.

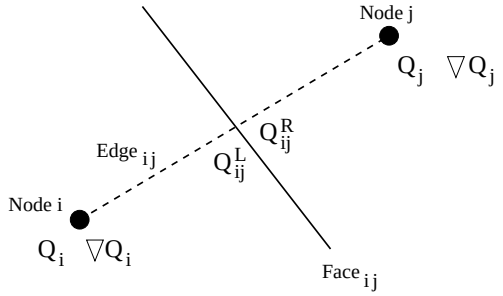

Figure 1. Typical edge and face within unstructured grid.

By setting $\phi = 1$ and $\chi = 0$ in the MUSCL-type scheme, using the assumptions that the least-squares gradient is equivalent to the central difference approximation to the gradient, the MUSCL-type scheme reduces to the classic unstructured variable extrapolation formula. This equivalence can be seen by starting

with Eqn. (1)

$$\begin{aligned} Q^L_{i+1/2} &= Q_i + \frac{1}{4}\left((1-0)\,\Delta_- + (1+0)\,\Delta_+\right) \\ &= Q_i + \frac{1}{4}\left(\Delta_- + \Delta_+\right) \\ &= Q_i + \frac{1}{4}\left(Q_i - Q_{i-1} + Q_{i+1} - Q_i\right) \\ &= Q_i + \frac{Q_{i+1} - Q_{i-1}}{4} \\ &= Q_i + \nabla Q_i \cdot \frac{\hat{r}}{2} \end{aligned} \tag{3}$$

In the following two sections, the original MUSCL-scheme is analyzed on uniform one-dimensional grids to show the order of accuracy of the scheme, and the Unstructured MUSCL (U-MUSCL) scheme is derived, which is applicable to unstructured flow solvers. Third order accuracy is demonstrated for a one-dimensional flow simulation, involving the St. Venant equations. Then, the reason that the overall scheme for unstructured grids can not be increased to third-order accuracy for two and three-dimensional grids by using the U-MUSCL approach is briefly discussed, although a reduction in numerical diffusion can be expected. Finally, the results of several three-dimensional simulations are shown, which demonstrate that the U-MUSCL scheme does significantly reduced the numerical diffusion and improves the ability to capture and maintain flow features.

II. MUSCL derivations

The extrapolation formula for the higher-order MUSCL schemes ($\phi = 1$) reduces to the following formula on uniform structured grids

$$Q^L_{i+1/2} = \frac{1+\chi}{4}Q_{i+1} + \frac{2-\chi}{2}Q_i + \frac{\chi-1}{4}Q_{i-1} \tag{4}$$

Expanding this expression about the extrapolation point $x_{i+1/2}$, it becomes

$$\begin{aligned} Q^L_{i+1/2} = &\frac{1+\chi}{4}\left(Q_{i+1/2} + Q'_{i+1/2}\frac{\Delta x}{2} + Q''_{i+1/2}\frac{\Delta x^2}{8} + Q'''_{i+1/2}\frac{\Delta x^3}{48} + O\left(\Delta x^4\right)\right) \\ &+\frac{2-\chi}{2}\left(Q_{i+1/2} - Q'_{i+1/2}\frac{\Delta x}{2} + Q''_{i+1/2}\frac{\Delta x^2}{8} - Q'''_{i+1/2}\frac{\Delta x^3}{48} + O\left(\Delta x^4\right)\right) \\ &+\frac{\chi-1}{4}\left(Q_{i+1/2} - Q'_{i+1/2}\frac{3\Delta x}{2} + Q''_{i+1/2}\frac{9\Delta x^2}{8} - Q'''_{i+1/2}\frac{27\Delta x^3}{48} + O\left(\Delta x^4\right)\right) \end{aligned} \tag{5}$$

which simplifies to

$$Q^L_{i+1/2} = Q_{i+1/2} + \frac{2\chi-1}{8}Q''_{i+1/2}\Delta x^2 + \frac{1-\chi}{8}Q'''_{i+1/2}\Delta x^3 + O\left(\Delta x^4\right) \tag{6}$$

Clearly, this formulation is at least second-order accurate. Furthermore, if χ is 1/2, then the variable extrapolation to the face is third-order accurate, and this formula is termed the "third-order variable extrapolation to the face". If χ is 1, then the Q''' term is zero, which has no upwinding and is not stable; and for any value of χ greater than 1, the formula is unstable, because of negative damping from the third order error term. The error terms for common and optimal choices of χ are shown in Table 1.

The finite volume method can be used to discretize the conservation law via the use of the divergence theorem

$$\int_{x_{i-1/2}}^{x_{i+1/2}} \frac{\partial F(Q)}{\partial x} dx = F(Q_{i+1/2}) - F(Q_{i-1/2}) \tag{7}$$

For simplicity, it will be assumed that $F(Q)$ is linear in Q. At this point, the expression is exact. When the values of Q at $x_{i-1/2}$ and $x_{i+1/2}$ are approximated via some extrapolation method, then discretization error

Table 1. Error Coefficients for Various Choices of χ based on Eqn. (5).

χ	$Q_i''\Delta x^2$	$Q_i'''\Delta x^3$	Comments
-1	-3/8	1/4	Second-Order MUSCL-type scheme
0	-1/8	1/8	Second-Order Unstructured (Eqn. (2))
1/3	1/24	1/12	Third-Order MUSCL-type scheme
1/2	0	1/16	Third-Order Extrapolation to Face
1	1/8	0	Central Difference Formula

is introduced. Assuming an upwind approach and using the values at the left sides of the faces, the MUSCL extrapolation method reduces to the following:

$$\begin{aligned}\int_{x_{i-1/2}}^{x_{i+1/2}} \frac{\partial Q}{\partial x} dx = Q_{i+1/2}^L - Q_{i-1/2}^L \approx &\left(\frac{1+\chi}{4}Q_{i+1} + \frac{2-\chi}{2}Q_i + \frac{\chi-1}{4}Q_{i-1}\right) \\ &- \left(\frac{1+\chi}{4}Q_i + \frac{2-\chi}{2}Q_{i-1} + \frac{\chi-1}{4}Q_{i-2}\right) \\ =&\frac{1+\chi}{4}Q_{i+1} + \frac{3-3\chi}{4}Q_i + \frac{3\chi-5}{4}Q_{i-1} + \frac{1-\chi}{4}Q_{i-2}\end{aligned} \tag{8}$$

Expanding this expression about the location x_i and reducing, one gets

$$\int_{x_{i-1/2}}^{x_{i+1/2}} \frac{\partial Q}{\partial x} dx = Q_i'\Delta x + \frac{3\chi-1}{12}Q_i'''\Delta x^3 + \frac{1-\chi}{8}Q_i''''\Delta x^4 + O(\Delta x^5) \tag{9}$$

Again, just as for the previous analysis, this formulation is second-order accurate for all choices of χ. If χ is 1/3, then the method is a third-order approximation to the derivative across the cell. If χ is 1, then the term associated with the third-order term is set to zero, as is the case for Eqn (6). This third-order term represents the leading-order diffusive term. When χ is one or greater, then this discretization becomes unstable due to the loss of this diffusive effect. The error terms for the approximation of the integral are shown in Table 2.

Table 2. Error Coefficients for Various Choices of χ based on Eqn. (8).

χ	$Q_i'''\Delta x^3$	$Q_i^{(iv)}\Delta x^4$	Comments
-1	-1/3	1/4	Second-Order MUSCL-type scheme
0	-1/12	1/8	Second-Order Unstructured (Eqn. (2))
1/3	0	1/12	Third-Order MUSCL-type scheme
1/2	1/24	1/16	Third-Order Extrapolation to Face
1	1/6	0	Central Difference Formula

From both extrapolations, Eqn. (6) and Eqn. (9), it is clear that the MUSCL scheme is at least second-order accurate for the variable extrapolation and the approximation of the first derivative when ϕ is set to 1. There is a discrepancy between whether third-order accuracy is achieved with χ is 1/3 or 1/2, which will be discussed in the following section and is demonstrated in the results.

III. Unstructured Extrapolation

As stated above, the information available to an edge-based unstructured flow solver for the calculations along the edge between nodes i and j are the flow values at the nodes and the gradients at the nodes. Hence,

the value extrapolated to the face can be stated in this general formula as

$$\tilde{Q}^L_{i+1/2} = Q_i + A\left(Q_j - Q_i\right) + B\nabla Q_i \cdot \frac{\hat{r}}{2} + C\nabla Q_j \cdot \frac{\hat{r}}{2} \tag{10}$$

The classic unstructured variable extrapolation formula, Eqn. (2), is achieved by setting $A = 0$, $B = 1$ and $C = 0$. Making the assumption of one-dimensional flow on a uniform grid, the edge is between nodes i and $i + 1$, and the formula becomes

$$\tilde{Q}^L_{i+1/2} = Q_i + A\left(Q_{i+1} - Q_i\right) + B\nabla Q_i \cdot \frac{\hat{r}}{2} + C\nabla Q_{i+1} \cdot \frac{\hat{r}}{2} \tag{11}$$

In one-dimension on a uniform grid, the least-squares approximation to the gradient for interior nodes results in a gradient equal to the central differences gradient, so that $\nabla Q_i \cdot \frac{\hat{r}}{2} = \frac{Q_{i+1} - Q_{i-1}}{4}$ and $\nabla Q_{i+1} \cdot \frac{\hat{r}}{2} = \frac{Q_{i+2} - Q_i}{4}$. Using these expressions, the variable extrapolation can be stated as

$$\tilde{Q}^L_{i+1/2} = \frac{C}{4}Q_{i+2} + \frac{4A + B}{4}Q_{i+1} + \frac{4 - 4A - C}{4}Q_i - \frac{B}{4}Q_{i-1} \tag{12}$$

This formula represents a three-parameter family, which under certain circumstances reduces to a two-parameter family that is second-order accurate. By setting C to zero, this formula reduces to a one-parameter family. The coefficient C is set to zero, because it multiplies the gradient on the opposite side of the face, which is a derived quantity and hence is probably the least reliable. Thus, the formula for approximating the derivative at the node is

$$\begin{aligned} \int_{x-1/2}^{x+1/2} \frac{\partial Q}{\partial x} dx &\approx \tilde{Q}^L_{i+1/2} - \tilde{Q}^L_{i-1/2} \\ &= \frac{4A + B}{4}Q_{i+1} + \frac{4 - 8A - B}{4}Q_i + \frac{4A - B - 4}{4}Q_{i-1} + \frac{B}{4}Q_{i-1} \end{aligned} \tag{13}$$

A. Variable Extrapolation to the Face

Using these expressions and expanding about the cell face at $x_{i+1/2}$, Eqn. (12) reduces to

$$\tilde{Q}^L_{i+1/2} = Q_{i+1/2} + \frac{2A + B - 1}{2}Q'_{i+1/2}\Delta x + \frac{1 - 2B}{8}Q''_{i+1/2}\Delta x^2 + \frac{2A + 7B - 1}{48}Q'''_{i+1/2}\Delta x^3 + O\left(\Delta x^4\right) \tag{14}$$

If $2A + B = 1$, then this extrapolation is higher-order accurate. Using this relationship, a one-parameter family which is second-order accurate results, or

$$\tilde{Q}^L_{i+1/2} = Q_{i+1/2} + \frac{4A - 1}{8}Q''_{i+1/2}\Delta x^2 + \frac{1 - 2A}{8}Q'''_{i+1/2}\Delta x^3 + O\left(\Delta x^4\right) \tag{15}$$

And if $A = 1/4$, then this extrapolation is third-order accurate, resulting in the following expansion

$$\tilde{Q}^L_{i+1/2} = Q_{i+1/2} + \frac{1}{16}Q'''_{i+1/2}\Delta x^3 + O\left(\Delta x^4\right) \tag{16}$$

Returning to equation (11), setting $A = 1/4$, $B = 1/2$ and $C = 0$, the third-order accurate expansion to the face is

$$\tilde{Q}^L_{i+1/2} = Q_i + \frac{1}{4}\left(Q_{i+1} - Q_i\right) + \frac{1}{2}\nabla Q_i \cdot \frac{\hat{r}}{2} \tag{17}$$

B. Approximation of the Derivative at the Node

Using the generalized formula Eqn. (13) for the approximation to the integral, this formula can be expanded about x_i to yield

$$\begin{aligned}\int_{x_{i-1/2}}^{x_{i+1/2}} \frac{\partial Q}{\partial x} dx \approx & \frac{4A+B}{4}\left(Q_i + Q_i'\Delta x + Q_i''\frac{\Delta x^2}{2} + Q_i'''\frac{\Delta x^3}{6} + Q_i''''\frac{\Delta x^4}{24} + O(\Delta x^5)\right) \\ & + \frac{4-8A-B}{4}\left(Q_i\right) \\ & + \frac{4A-B-4}{4}\left(Q_i - Q_i'\Delta x + Q_i''\frac{\Delta x^2}{2} - Q_i'''\frac{\Delta x^3}{6} + Q_i''''\frac{\Delta x^4}{24} + O(\Delta x^5)\right) \\ & + \frac{B}{4}\left(Q_i - Q_i' 2\Delta x + Q_i'' 4\frac{\Delta x^2}{2} - Q_i''' 8\frac{\Delta x^3}{6} + Q_i'''' 16\frac{\Delta x^4}{24} + O(\Delta x^5)\right)\end{aligned} \tag{18}$$

or

$$\int_{x_{i-1/2}}^{x_{i+1/2}} \frac{\partial Q}{\partial x} dx \approx Q_i'\Delta x + \frac{2A+B-1}{2}Q_i''\Delta x^2 + \frac{2-3B}{12}Q_i'''\Delta x^3 + \frac{2A+4B-1}{24}Q_i''''\Delta x^4 + O(\Delta x^5) \tag{19}$$

Again, a second-order accurate scheme for approximating the derivative at the node location is obtained by setting $2A + B = 1$, which is the same as above. However, a different third-order accurate family is obtained than the one presented above, by requiring that $A = 1/6$ and $B = 2/3$, with a leading order error term of $\frac{1}{12}Q_i''''\Delta x^4$. Using these values, Eqn. (12) results in the following third-order accurate formula

$$\int_{x_{i-1/2}}^{x_{i+1/2}} \frac{\partial Q}{\partial x} dx \approx Q_i + \frac{1}{6}\left(Q_{i+1} - Q_i\right) + \frac{2}{3}\nabla Q_i \cdot \frac{\hat{r}}{2} \tag{20}$$

As will be shown in the examples, however, Eqn. (20) does not yield third-order accuracy unlike Eqn. (17). The order of accuracy of Eqn. (20) is only second-order because of the second order error in the approximation of the integral with values at the node, or

$$\int_{x_{i-1/2}}^{x_{i+1/2}} \frac{\partial Q}{\partial x} dx = Q_i'\Delta x + Q_i'''\frac{\Delta x^3}{24} + O(\Delta x^5) \tag{21}$$

Actually, the third-order accurate formulation obtained when using this additional error term is the same as Eqn. (18). This conclusion differs from that presented in Anderson.[2]

C. Equivalence with MUSCL-type Scheme

The generalized formula, Eqn. (10), can be equated with the MUSCL-type scheme by comparing Eqn. (4) and (11). These two equations are equated by setting $A = \frac{\chi}{2}$, $B = (1 - \chi)$ and $C = 0$. Making the assumptions about uniform grids and the equivalence of the gradient calculated via Green-Gauss or Least-Squares with a central difference gradient, the generalized formula for the unstructured grids that equates to the MUSCL-type scheme is the following:

$$\tilde{Q}_{i+1/2}^{L} = Q_i + \frac{\chi}{2}\left(Q_{i+1} - Q_i\right) + (1-\chi)\nabla Q_i \cdot \frac{\hat{r}}{2} \tag{22}$$

If χ is set to 0, then the original unstructured formulation for second-order variable extrapolation is obtained. If χ is set to -1, then the second-order fully-upwinded MUSCL-type variable extrapolation is obtained. If χ is set to 1/2, a third-order variable extrapolation to the cell face is achieved which is equivalent to Eqn (17), while if χ is set to 1/3, a third-order approximation to the derivative at the node is achieved, which reduces to Eqn (20). This formula is an upwind formula as long as $\chi < 1$ and as such is stable for hyperbolic systems of equations that do not contain shocks and for good quality grids.

IV. One-Dimensional St. Venant Equations

The one-dimensional St. Venant Equations represent a simplification of the incompressible Navier-Stokes equations as applied to open-channel flow and can be expressed in the following form, ignoring friction and the effects of bed slope

$$\begin{aligned} \frac{\partial h}{\partial t} + \frac{\partial p}{\partial x} &= 0 \\ \frac{\partial p}{\partial t} + \frac{\partial}{\partial x}\left(\frac{p^2}{h} + \frac{1}{2}gh^2\right) &= 0 \end{aligned} \tag{23}$$

where h is the depth of flow and p is the discharge rate. A node-centered finite volume scheme including the use of Roe-averaged variables is used to discretize these equations.[6] A modified system of governing equations is obtained via Roache's method of manufactured solutions[7] by applying the spatial terms to a manufactured solution which in this case is the following:

$$\begin{aligned} h(x) &= e^{-x/A} \\ p(x) &= e^{x/A} \end{aligned} \tag{24}$$

where A is the length of the channel. The resulting equations are added to the right-hand-side and act as source terms that drive the solution towards the manufactured solution. The modified equations can be stated as

$$\begin{aligned} \frac{\partial h}{\partial t} + \frac{\partial p}{\partial x} &= \frac{1}{A}e^{x/A} \\ \frac{\partial p}{\partial t} + \frac{\partial}{\partial x}\left(\frac{p^2}{h} + \frac{1}{2}gh^2\right) &= \frac{3}{A}e^{3x/A} + \frac{g}{2A}e^{-2x/A} \end{aligned} \tag{25}$$

The right-hand-side is discretized in the same fashion as the left by integrating over the control volume and evaluating the result at the boundary of the control volume. This process is simplified by the use of a symbolic manipulation software such as *Mathematica*.

Furthermore, it can be shown that by plugging the manufactured solution into the modified code, the values for the discretized equations is the local truncation error of the discretization method.[8] The results shown in Table 3 are the L1-norm of the local truncation error for the interior nodes for a sequence of grids.

Table 3. L1-Norm of Local Truncation Error for St. Venant Equations Code. ($\times 10^4$)

Grid	Nodes	$\chi = -1$	$\chi = 0$	$\chi = 1/3$	$\chi = 1/2$	$\chi = 9/10$
1	101	7.213347	2.381005	0.770225	0.03516544	1.968102
2	201	1.806126	0.599134	0.196803	0.00436223	0.487159
3	401	0.451864	0.150259	0.049724	0.00054320	0.121185
4	801	0.113007	0.037624	0.012496	0.00006777	0.030221
5	1601	0.028257	0.009413	0.003132	0.00000846	0.007546
6	3201	0.007065	0.002354	0.000784	0.00000106	0.001885

This table clearly demonstrates that the local truncation error is smaller for the choices of 1/3 and 1/2 than for the classic unstructured variable extrapolation formula and that the choice of $\chi = 1/2$ yields third-order accurate results for the local truncation error. This table also shows that the error is larger for $\chi = -1$ which corresponds to the traditional structured second-order formula and for $\chi = 9/10$ which is close to the limit of stability for this method.

In Table 4, the L1-norm between the solution at the nodes and the exact solution at these locations is compared for the various choices of χ. As was seen with the local truncation error, the error in the solution at the nodes demonstrates second-order convergence in that when the grid is refined by a factor of 2, the

Table 4. L1-Norm of Error between Exact and Converged Solutions for St. Venant Equations Code ($\times 10^4$)

Grid Level	Nodes	$\chi = -1$	$\chi = 0$	$\chi = 1/3$	$\chi = 1/2$	$\chi = 9/10$
1	101	12.4156903	4.1685414	1.3843028	0.029287578	3.5541471
2	201	3.1060677	1.0337583	0.3427514	0.003616659	0.8400250
3	401	0.7767949	0.2588370	0.0860787	0.000452452	0.2080108
4	801	0.1942341	0.0647337	0.0215540	0.000056556	0.0518638
5	1601	0.0485630	0.0161863	0.0053924	0.000007069	0.0129591
6	3201	0.0121413	0.0040469	0.0013486	0.000000884	0.0032389

error is reduced by a factor of 4. For $\chi = 1/2$, however, the convergence rate is third-order since the error reduces by approximately 8 when the grid is refined by a factor of 2. According to the MUSCL-type scheme,[2] however, the third-order scheme should be obtained when $\chi = 1/3$. For this example, the third-order scheme is clearly obtained when $\chi = 1/2$. The primary reason for this difference is that the analysis that led to the conclusion that $\chi = 1/3$ is third-order makes the assumption that the scheme is approximating the derivative at the node, whereas the scheme is actually approximating the value at the face.

V. Extensions to Higher Dimensions

The U-MUSCL variable extrapolation formula has been demonstrated to be third-order accurate when $\chi = 1/2$ for extrapolating to the face of the control volume. In one-dimension, this extrapolation yields a scheme that is third-order accurate overall for a uniform grid, as demonstrated for the St. Venant case presented in the previous section. However, for higher dimensions and for non-uniform grids, there are several other approximations for the standard unstructured finite volume methodology, which are first and second-order accurate. In fact, the typical unstructured finite volume implementation for non-uniform unstructured grids is technically only first-order accurate, due to several sources, which include

1. The center of control volume does not coincide with the nodal location for node-centered finite volume methods.

2. The center of the face of the control volume does not lie halfway between the adjoining cell centroids for cell-centered finite volume methods.

3. The centers of the faces do not coincide with the location to which the values are extrapolated.

These cases are illustrated in Figures 2 and 3. In Figure 2, a cell-centered discretization is shown, which illustrates that the face of the cell may not lie halfway between the adjoining cell-centroids. In Figure 3, a node-centered discretization is shown. The open circles represent the centroids of the control volumes, which do not coincide with the nodes, and the midpoint of the edge connecting the two nodes does not coincide with the center of the common face. Each of these distortions introduces a reduction in the order of the discretization to first-order. However, these influences are so small that they are not detectable for good quality grids.

In the ideal unstructured grid, the variables are extrapolated to the center of the control volume face. As such, a one-point interpolation of the surface integral will be second-order accurate. If the variables are extrapolated to a different location, then the one-point interpolation is only first-order accurate. However, this first order error term is a function of the distance between the optimal location and the extrapolated location, which should be quite small for good quality grids. Similarly, the other issues involved in the discretization including the difference between the center of the control volume and the location from which the values are stored and extrapolated introduce first-order errors into the discretization. These again are a function of the distance between the centroid of the control volume and the nodal location. As such, these errors are orders of magnitude smaller than the second-order error terms, and are not typically identifiable.

Even on a uniform grid, the one-point interpolation to the face of the control is at best only second-order accurate, and can not be extended to third-order accuracy. Hence, having a third-order accurate extrapola-

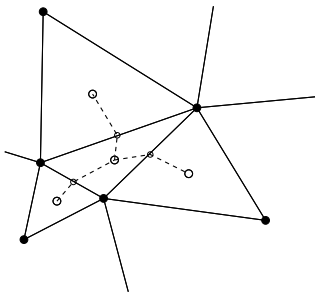

Figure 2. Example of Distorted Cell-Centered Finite Volume Grid

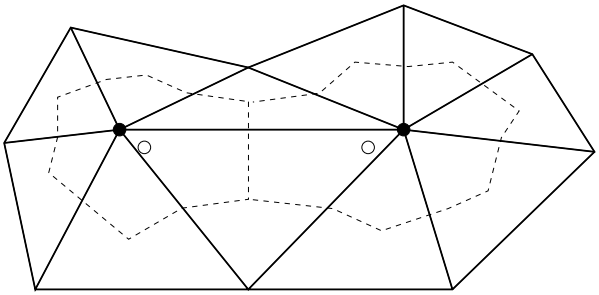

Figure 3. Example of Distorted Node-Centered Finite Volume Grid

tion to the face will not yield a third-order accurate result, because of this single-point face integration. As an example, the U-MUSCL variable extrapolation method was applied to a two-dimensional unstructured RANS code,[9] which had been verified via the residual form of the method of manufactured solutions.[8] On a uniform grid, consisting of equilateral triangles, the error in the continuity equation residual decreases at a second-order rate for all values of χ, as is shown in Table 5. However, for $\chi = 1/2$, the error dips significantly below the other errors for the other choices of χ, indicating that the improved extrapolation for $\chi = 1/2$ has a significant influence in reducing the errors, even though the order of accuracy does not change.

Table 5. Error ($\times 10^{10}$) in Continuity Equation for 2D RANS Solver on Uniform Equilateral Triangular Mesh

Triangles	$\chi = 0$	$\chi = 1/3$	$\chi = 1/2$	$\chi = 2/3$	$\chi = 0.8$
64	3782.843	1347.583	129.954	1087.676	2061.780
256	1183.945	422.300	41.477	339.345	644.003
1024	327.951	117.051	11.601	93.849	178.209
4096	86.115	30.742	3.055	24.631	46.780

VI. Three-Dimensional RANS Solver

The U-MUSCL variable extrapolation scheme has been implemented within the unstructured viscous incompressible flow solver U^2NCLE, which uses flux-differencing and Roe-averaged variables to approximate the convective fluxes for the Reynolds-averaged Navier-Stokes equations and uses a directional derivative approach to discretized the viscous terms of the equations. The interested reader is referred to the AIAA paper by Hyams.[10] This flow solver has been validated for steady-state and time-accurate flows for complicated geometries,[11–13] and a preliminary verification of second-order accurate implementation has been completed[14]

A. Prolate Spheroid Simulations

The prolate spheroid is a body of revolution which in this case is defined by the equation

$$\frac{x^2}{36} + y^2 + z^2 = \frac{1}{144} \tag{26}$$

Several different types of grids were generated in this study, including a tetrahedra grid with uniform point spacings, a series of tetrahedral grids with typical point spacings for this type of geometry and a viscous, mixed element grid. The grid with uniform point spacing was used to determine the influence of the non-uniformity in a typical grid on the performance of the U-MUSCL variable extrapolation method. The series of tetrahedral grids were used for a grid refinement study, to demonstrate the second order convergence of the inviscid flow solver, for which the drag should be zero since the geometry is streamlined. The viscous grid was used to complete the study, showing the effects of the U-MUSCL scheme, which only deals with the inviscid component of the flow solver, on a viscous simulation.

These grids were generated from an unstructured, triangular surface grid using Marcum's AFLR3 grid generation package[15] to create the specific type of volume grid. For the tetrahedral grids, no boundary layer was built, which is acceptable since only an inviscid simulation would be performed. In a related grid refinement study, it was demonstrated that the unstructured flow solver produced zero side forces and moments when a symmetric unstructured grid was built by reflecting a fully-unstructured grid in one octant about the planes of symmetry.[14] In this example, however, neither the surface nor volume grids were built to guarantee symmetry in the grid about the coordinate directions.

B. Inviscid Prolate Spheroid

A grid refinement study was performed on the prolate spheroid, along with a study of the U-MUSCL parameter. Three unstructured grids were built and are described in Table 6. In these grids, the grid spacing was reduced by a factor of 2 each time rather than performing an h-refinement starting with the first grid. As a result, the number of tetrahedra did not increase by a factor of 8 with each refinement, being approximately a factor of 4 for the first grid level to the next, a factor of 6 for the next set and a factor of 11 for the final set.

Table 6. Number of Nodes and Tetrahedra in Grid Sequence for Prolate Spheroid

Grid Level	Nodes	Tetrahedra
1	27,525	153,309
2	112,256	626,121
3	678,222	3,860,416
4	7,729,750	45,116,795

By running the three-dimensional unstructured flow solver without the viscous terms, the code solved the Euler equations which should produce a drag of 0.0, because the body was streamlined. Hence any drag that is produced by the code is a measure of the numerical viscosity introduced into the simulation by the discretization error. Furthermore, since the analytic value of drag is known, this test case also acts as a verification that the discretization for tetrahedral grids is second-order accurate. The drag predicted by the unstructured flow solver U^2NCLE is given in Table 7. In comparison with $\chi = 0$ which represents the classic unstructured variable extrapolation, the drag induced by numerical viscosity is approximately 30 % less for $\chi = 1/3$ and is approximately 47 % for $\chi = 1/2$, while the drag coefficient predicted by $\chi = 0.95$ is an order of magnitude smaller than for $\chi = 0$.

The drag continues to decrease as χ increases towards 1.0, getting quite close to zero. However, as χ gets close to 1.0, the convergence rate decreases and for $\chi = 1$, the simulation diverges.

C. Nearly Uniform Grid for Prolate Spheroid

For the 1D and 2D cases, the optimal observed value for the U-MUSCL parameter was 0.5, which agrees with the theoretical optimum. However, for all of the 3D cases, both inviscid and viscous, the optimal value of the

Table 7. Drag Coefficient Predictions for Prolate Spheroid ($\times 10^6$).

Grid	$\chi = 0$	$\chi = 1/3$	$\chi = 1/2$	$\chi = 0.6$	$\chi = 0.7$	$\chi = 0.8$	$\chi = 0.9$	$\chi = 0.95$
1	345.8009	250.0597	198.0972	165.0681	130.1936	92.8788	52.2264	30.6311
2	70.3592	48.7002	37.4753	30.5756	23.5206	16.2647	8.7228	4.8868
3	11.4578	7.9008	6.0761	4.9646	3.8356	2.6810	1.4833	0.8617
4	2.8413	1.9547	1.5058	1.2335	0.9582	0.6781	0.3907	0.2449

U-MUSCL extrapolation parameter is the closest value to 1.0 that remains stable without the use of limiters. Several possible reasons for this change in behavior need to be investigated, including the non-uniformity of elements and point spacings within unstructured grids. For the 2D case, the extrapolation scheme was tested on a perfectly uniform equilateral triangular grid. As a result, the least-square gradient was exactly second-order accurate, as were the other discretizations within the flow solver. However, for the 3D cases, the grids were not perfectly uniform, which introduces error into the least-squares gradient as well as the other components of the discretization.

In an effort to investigate the effects of the non-uniformity, an unstructured grid was built about the prolate spheroid where the spacing was the same for all of the control points within the geometry, which meant that the elements were roughly the same size throughout the domain. However, because of the nature of unstructured grids, the grid would not be perfectly uniform. The drag coefficient for this inviscid simulation, which should be zero, is shown in Table 8.

Table 8. Drag Coefficient for Nearly Uniform grid about Prolate Spheroid ($x10^4$).

U-MUSCL Value	0.0	0.2	0.4	0.5	0.6	0.8	0.9	0.95
Drag Force Coef.	5.599	5.238	4.758	4.449	4.070	2.940	2.004	1.358

Rather than achieving the minimum drag value at $\chi = 0.5$, the minimum value was obtained as χ approaches its stability limit near $\chi = 1.0$. This behavior was mitigated by the use of a nearly uniform unstructured grid because the reduction in the drag coefficient from $\chi = 0.0$ to $\chi = 0.95$ was only a factor of 4, rather than a factor of 10 or more, as was seen in the inviscid prolate spheroid case.

D. Viscous Prolate Spheroid

The same type of study was applied to a viscous prolate spheroid, where the grid was constructed to be symmetric in all three directions. The grid is a viscous grid consisting of approximately 1.5 million nodes, and the simulation is performed at a Reynolds number of 4.2 million. The drag for this geometry and for these conditions is shown in Figure 4 , showing the variation of the drag with respect to the U-MUSCL parameter. As χ increases towards 1.0, the drag monotonically decreases, indicating that the numerical dissipation is decreasing. Because the grid is high quality and the flow is relatively calm, the simulation is stable enough that no limiters were needed, even for $\chi = 0$ and for $\chi = 0.95$. Clearly from this figure, the minimum will occur after $\chi = 0.95$. However, for more complicated simulations, as χ approaches 0 or 1, the flow solver typically becomes less stable, requiring the use of a limiter, which will increase the numerical dissipation and thus the drag.

E. Inviscid DTMB Model 5415 Results

The first inviscid grid that was used for the rigid lid simulation about the David Taylor Model Basin (DTMB) Model 5415 was a fully tetrahedra grid consisting of 309,163 nodes. For this grid, the value of χ was varied from -1 to 0.95, with the drag calculated for each value of χ given in Table 9. Since the flow is inviscid, the drag should be zero, if the geometry is streamlined. However, the stern region is a transom, which contains a region of recirculation, so that the drag is a small nonzero quantity for this geometry.

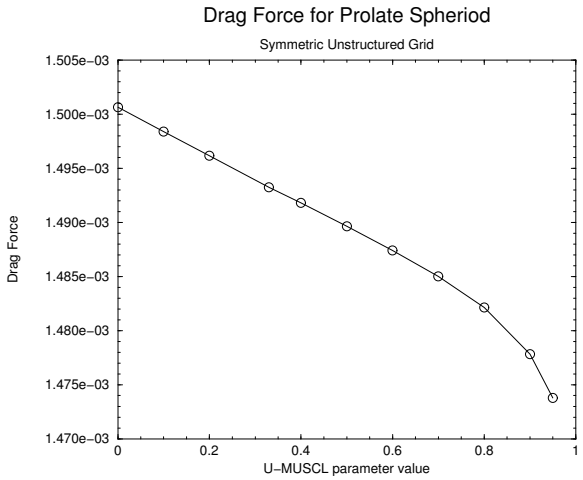

Figure 4. Variation of Drag with respect to U-MUSCL parameter for Prolate Spheroid

Table 9. Drag Coefficient for Inviscid Simulation about DTMB Model 5415. ($x10^5$)

χ	-1.0	0.0	0.1	0.2	0.3	0.4	0.5	0.6	0.7	0.8	0.9	095
Drag Coef.	12.16	8.30	7.97	7.62	7.24	6.83	6.39	5.93	5.46	5.16	7.00	7.50

The simulation is stable and converges to machine precision for values of χ between 0.0 and 0.8, but requires a limiter to maintain stability for $\chi = -1$ and for χ above 0.8. As has been shown above, the drag coefficient, which is small but positive, decreases monotonically from 0.0 to 0.8, with a significant variation across this range of parameters.

F. Viscous DTMB Model 5415 Simulations

For the viscous DTMB Model 5415 simulations, the Spalart-Allmaras turbulence model was chosen, and five values of χ were studied. For $\chi = 1/3$, $\chi = 1/2$ and $\chi = 5/6$, the solutions were strongly convergent, while the convergence level stagnates for the choice of $\chi = 0$, which has been seen for most turbulent, viscous simulations. It also stagnates for $\chi = -1$ and requires a limiter for stability. Being able to drive the solution to machine precision for a turbulent, viscous simulation is remarkable, considering the complexity of the flow physics. The drag predicted by each simulation is tabulated below in Table 10. When $\chi = 0$ or $\chi = -1$, edge-based limiting was used to maintain stability of the algorithm, which artificially increased the drag coefficient. Regardless of this influence, the drag tended to decrease as χ increased towards 1/2, as has been shown before.

Table 10. Drag Calculated for Naval Destroyer Hull Form (x10^4)

χ	-1	0	1/3	1/2	5/6
Drag Coefficient	4.6219	4.6179	4.4950	4.4826	4.5350

The simulation was also run with a value of $\chi = 1$, which reduces to a central difference approximation with no upwinding. However, for this value of χ, the simulation was unstable, gradually diverging after 1000's of iterations.

When $\chi = 0$, some sort of limiting is needed to maintain stability, which in this case involved edge-based limiting. Starting with the converged solution and turning off the edge-based limiting, the solution diverged within 200 iterations. When $\chi = -1$, again edge-based limiting was employed and the solution was not

strongly convergent, and stalled at the same level of convergence as for $\chi = 0$.

Hence, from the perspective of obtaining a strongly convergent solution without the need for limiters, values of χ in the range from 0 to 1, not inclusive, appear to allow strongly convergent solutions. Values in this range produce a formulation that has positive coefficients for edge-based gradient based on the difference in the values at the nodes and for the gradient calculated at node i, as can be seen from the U-MUSCL scheme

$$\tilde{Q}^L_{i+1/2} = Q_i + \frac{\chi}{2}\left(Q_{i+1} - Q_i\right) + (1-\chi)\nabla Q_i \cdot \frac{\hat{r}}{2} \tag{27}$$

Furthermore, for values of χ greater than 1, the truncation error indicates that the coefficient for the diffusive fourth-order error term would become negative, indicating negative diffusivity which is typically unstable.

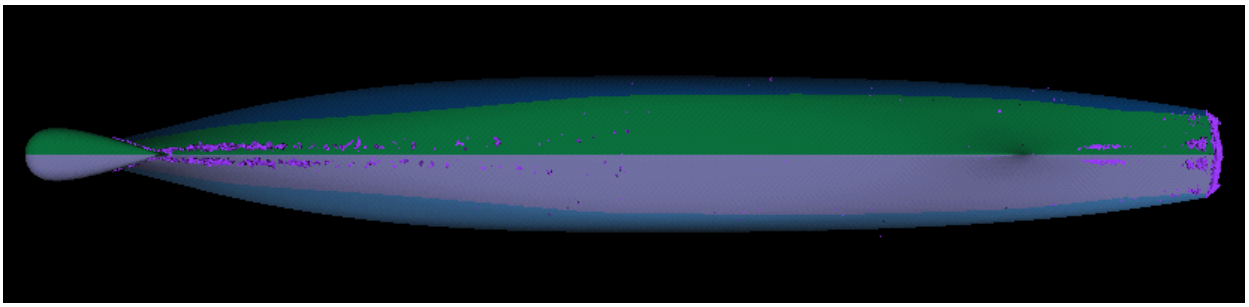

Figure 5. Vortical Structures for Naval Destroyer for $\chi = 0$

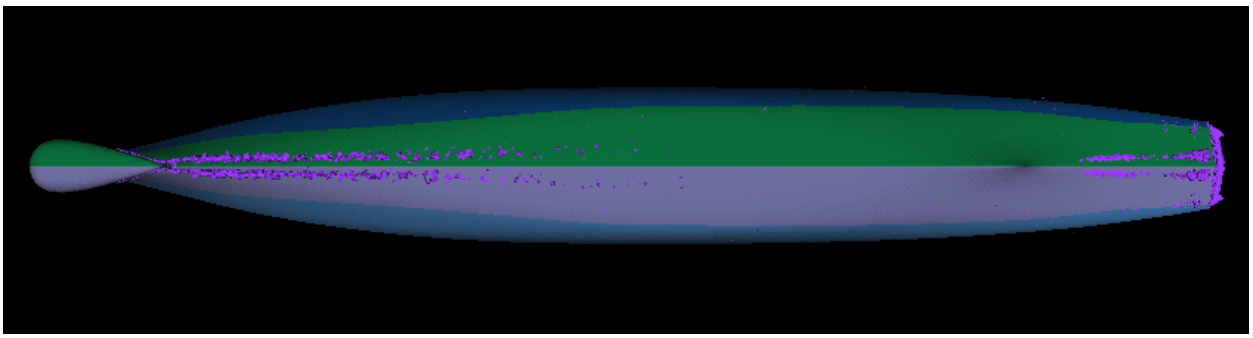

Figure 6. Vortical Structures for Naval Destroyer for $\chi = 1/3$

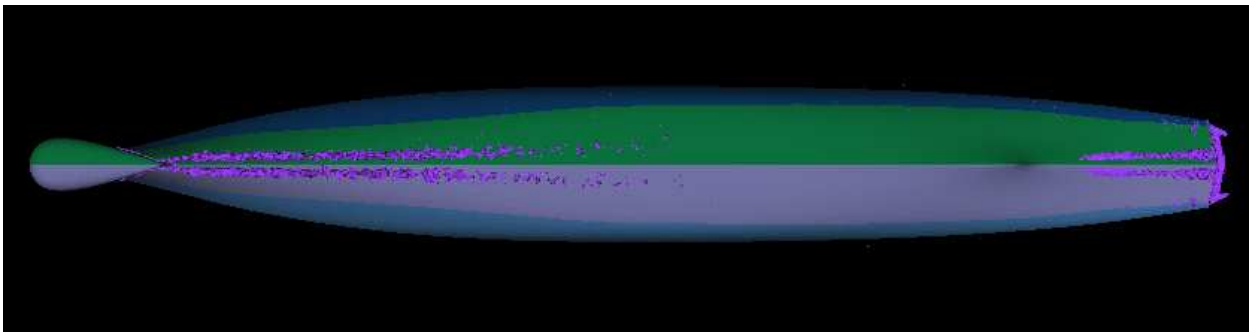

Figure 7. Vortical Structures for Naval Destroyer for $\chi = 1/2$

An additional benefit of the Unstructured-MUSCL variable extrapolation formulation is that the vortical structures are convected further downstream than with the previous extrapolation method. This benefit is a direct result of the decreased numerical viscosity, and can be seen in the vortices that arise from the bulbous bow and the stern region. As would be expected, as χ increases towards 1/2, these vortices are more clearly resolved, as are shown in Figures 5, 6, and 7.

G. Modified Kriso Very Large Container Ship KVLCC2M

A more rigorous grid refinement was performed on the KVLCC2M hullform, which is a slightly modified version of the Kriso Very Large Container Ship. This geometry was constructed so that the grids were symmetric about the symmetry plane. Furthermore, great care was exercised to generate almost geometrically similar unstructured grids. The boundary layer grid was built via extrusion of the nodes on the viscous so that the number of prismatic layers could be controlled, as well as the thickness of each prismatic layer and the total thickness of the boundary layer grid. For these grids, the thickness of the prismatic boundary layer was the same, and the number of layers and thickness of each layer varied based on the grid refinement ratio. Then, the remainder of the volume grid was filled with tetrahedra. The number of prisms, tetrahedra and nodes in the each grid are presented in Table 11. The refinement ratio was $\sqrt{2}$, which should increase the total number of nodes by a factor of $2\sqrt{2}$ in each grid refinement.

Table 11. Grid Information for KVLCC2M Refinement Study.

Grid Level	Prisms	Tetrahedra	Nodes
1	297,800	655,908	274,651
2	838,880	1,692,990	735,111
3	2,420,880	4,478,652	2,026,521
4	6,759,928	12,314,450	5,579,251

The data for the KVLCC2M hullform is shown in in Table 12. For values of χ between 0.2 and 0.8 and many of the other values and grids, the results are quite consistent, monotonically decreasing with χ, with a meaningful order of accuracy. The order of accuracy calculation requires data from three grids, so two different sets of calculations can be performed. For those dealing with the three least resolved grids, the order of accuracy decreases with χ, but for those dealing with the three most resolved, the order increases with χ. The overall methodology is approximately second-order accurate, with the appropriate caveats for finite volume solvers on unstructured grids. As the grid size tends to zero, the order of accuracy appears to be converging towards zero.

Table 12. Drag for KVLCC2M hullform ($x10^3$).

U-MUSCL	Grid 1	Grid 2	Grid 3	Grid 4	Order 123	Order 234
0.0	1.167589593	1.092070486	1.057346438	0.987406180	2.242	NM
0.1	1.158583264	1.088707139	1.073729645	0.549696867	4.444	NM
0.2	1.149536238	1.085466613	1.066465510	1.056390706	3.507	1.831
0.3	1.140550634	1.082375312	1.064205588	1.055611871	3.357	2.160
0.4	1.130710575	1.078894671	1.062998615	1.054988517	3.410	1.978
0.5	1.122736409	1.076720909	1.061734001	1.054361018	3.237	2.047
0.6	1.114818787	1.074771880	1.060501950	1.053657720	2.978	2.120
0.7	1.106805940	1.073053337	1.059210599	1.052768052	2.572	2.207
0.8	1.097756210	1.071523934	1.057726385	1.051446459	1.854	2.271
0.9	1.084459790	1.069333700	1.055070231	1.048869887	NM	2.404
0.95	1.077920952	1.066729493	1.051443133	1.046268106	NM	3.125

A plot of these results in shown in Figure 8. A limiter was required for convergence for the finest grid

when $\chi = 0.0$ or 0.1, which significantly altered the results. The slope for the coarse grid (Grid 1) is more than the others, showing a greater influence on the χ parameter. In addition, as has been seen above, the drag reduction accelerates as χ near a value of 1.0. Both of these observations can account for the variation in the order of accuracy.

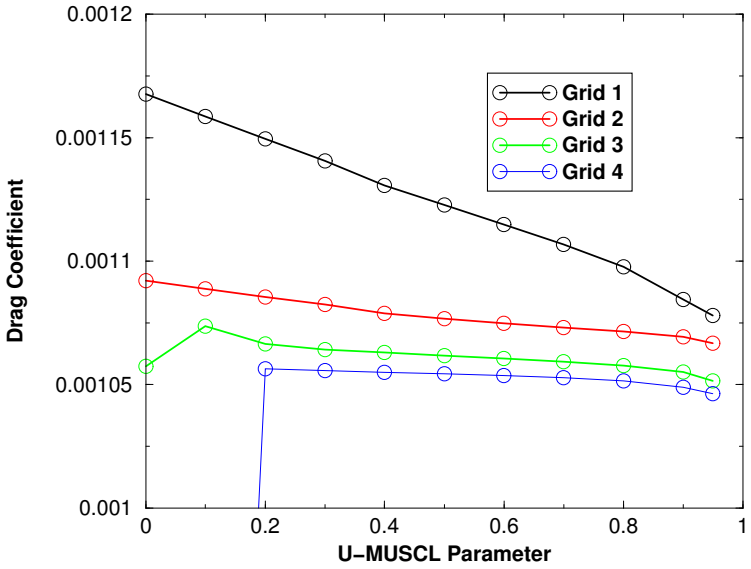

Figure 8. Drag Coefficient for KVLCC2M for different grids and different U-MUSCL values.

H. Rudder Simulations

The final example deals with a rudder at various angles of attack. This rudder comes from a naval destroyer class vessel, for which experimental data exists for the drag calculations. This rudder is symmetric, so that the lift coefficient should be zero for zero degrees angle of attack simulations. Since no effort was made to build a symmetric grid, the variation from zero is a direct result of numerical errors. The lift coefficient for zero angle of attack is shown in Table 13. Two different grids were built, a coarse and a refined grid, and two different values of χ were used in the simulations. As the grid is refined and for the optimal value of χ, the lift is closer to zero.

Table 13. Lift Coefficient (x10^4) for Symmetric Flow Across Symmetric Rudder

Simulation	Lift Coef.
Coarse Grid ($\chi = 0$)	-8.39647434728
Coarse Grid ($\chi = 1/2$)	-7.46091405175
Refined Grid ($\chi = 1/2$)	-3.69159729175

Also, since experimental data is available for the drag coefficient at several angles of attack, the same combinations of grids and χ were compared with the experimental data for the drag coefficient, which is shown in Figure 9. As the grid is refined and for optimal choice of χ, the drag coefficient agrees more closely with the experimental data, demonstrating that the U-MUSCL variable extrapolation method is less diffusive and hence adds less numerical dissipation to the simulations.

VII. Conclusions

The Unstructured MUSCL variable extrapolation formulation has been presented, which offers the potential for third-order variable extrapolation to the face of control volumes. Under certain circumstances, such

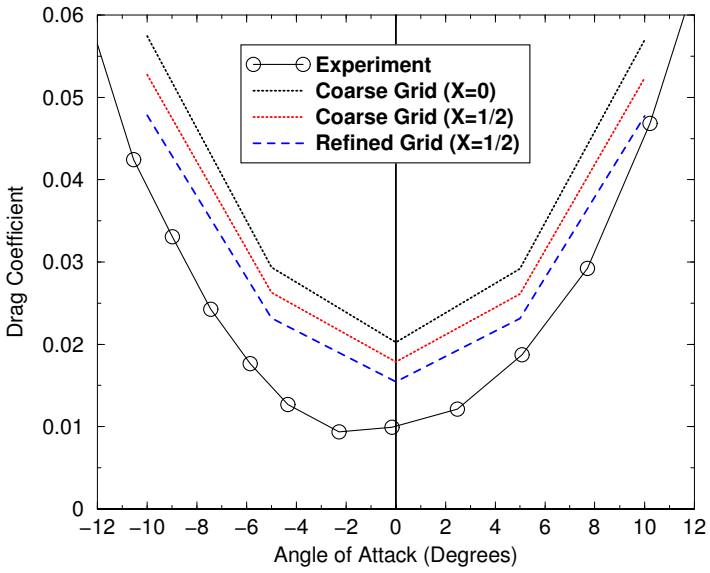

Figure 9. Drag Coefficient for Rudder of Naval Destroyer

as simulations on uniform grids, this formulation is exactly equal to van Leer's MUSCL formulation. This formulation will not yield third-order accurate discretizations for two-dimensional and three-dimensional grids, due to other first and second-order approximations within these discretizations, but the use of the improved variable extrapolation significantly reduces the numerical viscosity, as is evidenced by improved coefficient calculations for viscous and inviscid flows and by better resolution of vortical structures within the flowfield.

The U-MUSCL scheme was tested on a one-dimensional open-channel flow simulation and was shown to yield third-order error reduction, as the grid was resolved. This scheme was incorporated into a 2D RANS solver, as well as a mature 3D RANS solver. For the 2D solver, the error in the simulation was reduced significantly when $\chi = 1/2$, even though third-order accuracy was not achieved.

Results from several different 3D unstructured simulations were presented. Inviscid flow about a symmetric prolate spheroid was shown to yield a positive non-zero drag, which was a result of numerical viscosity within the simulation. As the grid was refined and the value of χ was increased towards 1, the drag coefficient reduced towards the theoretical value of zero. Inviscid and viscous simulations about a typical naval destroyer and about a typical container ship were also performed, showing that the force coefficients tended towards zero as χ increased towards 1 for the inviscid cases. The viscous simulations showed that the drag coefficient was the least for the largest value χ for which the flow solver was fully stable. For the viscous case, the residual could be driven to machine zero for values of χ between 0 and 1, and the vortical structures within the flow were better resolved for $\chi = 1/2$. Finally, similar performance improvements were seen with the viscous flow simulations about a rudder, at various angles of attack.

Overall, the U-MUSCL formulation is easy to implement within most unstructured flow solvers and yields better numerical results due to reduced numerical diffusion. In addition, for the incompressible RANS code tested herein, the U-MUSCL scheme resulted in much more stable simulations. Additional research is required to understand why the U-MUSCL scheme is more stable than the typical unstructured extrapolation scheme for viscous cases and why the optimal value of χ for the three-dimensional simulations differs from the theoretical optimum.

References

[1]Van Leer, B., "Towards the Ultimate Conservative Difference Scheme, V. A Second Order Sequel to Godunov's Method", *J. Comput. Physics*, Vol. 32, 1979, pp. 101-136.

[2]Anderson, W. K., Thomas, J. L., and Van Leer, B., "Comparison of Finite Volume Flux Vector Splittings for the Euler Equations", AIAA J., Vol. 24, No. 9, Sept. 1986, pp. 1453-1460.

[3]Janus, J. M., and Whitfield, D. L., "A Simple Time-Accurate Turbomachinery Algorithm with Numerical Solutions of an Uneven Blade Count Configuration", AIAA Paper 89-0206, Jan. 1989.

[4]Pankajakshan, R. Taylor, L. K., Jiang, M., Remotigue, M. J., Briley, W. R., and Whitfield, D. L., "Parallel Simulations for Control-Surface Induced Maneuvers", AIAA Paper 2000-0962, Jan. 2000.

[5]Barth, T. J., and Jespersen, D. C., "The Design and Application of Upwind Schemes on Unstructured Meshes", AIAA Paper 89-0366, 27th Aerospace Sciences Meeting, Jan., 1989, Reno. NV.

[6]Whitfield, D. L., "Numerical Solution of the Shallow Water Equations", MSU Report MSSU-EIRS-ERC-96-4, July, 1996.

[7]Roache, P. J., *Verification and Validation in Computational Science and Engineering*, Hermosa Publishers, Albuquerque, 1998.

[8]Burg, C. O. E., Murali, V. K., "Efficient Code Verification Using the Residual Formulation of the Method of Manufactured Solutions", AIAA Paper 2004-2628, 34th AIAA Fluid Dynamics Conf., June, 2004, Portland, Oregon.

[9]Murali, V. K., Burg, C. O. E., "Verification of 2D Navier-Stokes Codes by the Method of Manufactured Solutions", AIAA Paper 2002-3109, 32nd AIAA Fluid Dynamics Conf., June, 2002, St. Louis.

[10]Hyams, D. G., Sreenivas, K., Sheng, C., Briley, W. R., Marcum, D. L., and Whitfield, D. L., "An Investigation of Parallel Implicit Solution Algorithms for Incompressible Flows on Multielement Unstructured Topologies", AIAA Paper 2000-0271, 39th AIAA Aerospace Sciences Meeting ', Jan. 2000, Reno, NV.

[11]Blades, E., Marcum, D., and Mitchell, B., "Simulation of Spinning Missile Flow Fields Using U2NCLE", AIAA Paper 2002-2797, 32nd AIAA Fluid Dynamics Conference, June, 2002, St. Louis.

[12]Sreenivas, K., Hyams, D., Mitchell, B., Taylor, L., Marcum, D. and Whitfield, D. "Computation of Vortex-Intensive Incompressible Flow Fields", AIAA Paper 2002-3306, 32nd AIAA Fluid Dynamics Conference, June, 2002, St. Louis.

[13]Burg, C. O. E., Sreenivas, K., Hyams D., and Mitchell, B., "Unstructured Nonlinear Free Surface Flow Solutions: Validation and Verification", AIAA Paper 2002-2977, 32nd AIAA Fluid Dynamics Conference, June, 2002, St. Louis.

[14]Burg, C. O. E., Sheng, C., Newman, J. C. III, Brewer, W., Blades, E., and Marcum, D. L., "Verification and Validation of Forces Generated by an Unstructured Flow Solver", AIAA Paper 2003-3983, 16th AIAA Computational Fluid Dynamics Conf., June, 2003, Orlando, FL.

[15]Marcum, D. L. "Unstructured Grid Generation Using Automatic Point Insertion and Local Reconnection", The Handbook of Grid Generation, editted by J. F. Thompson, B. Soni and N. Weatherill, CRC Press, 1998, Section 18.